Geofluids (2004) **4**, 329–340

The Ixtacamaxtitlán kaolinite deposit and sinter (Puebla State, Mexico): a magmatic-hydrothermal system telescoped by a shallow paleoaquifer

J. TRITLLA[1], A. CAMPRUBÍ[1], J. M. MORALES-RAMÍREZ[1], A. IRIONDO[1,2], R. CORONA-ESQUIVEL[3], E. GONZÁLEZ-PARTIDA[1], G. LEVRESSE[1] AND A. CARRILLO-CHÁVEZ[1]

[1]*Centro de Geociencias, Universidad Nacional Autónoma de México, Santiago de Querétaro, Querétaro, Mexico;*
[2]*Department of Geological Sciences, University of Colorado at Boulder, Boulder, CO, USA;*
[3]*Instituto de Geología, Universidad Nacional Autónoma de México, Ciudad Universitaria, México DF, Mexico*

ABSTRACT

The Ixtacamaxtitlán hydrothermal deposit is made up of a succession, from bottom to top, of: (1) a porphyritic subvolcanic body, crosscut by quartz veins, and a stockwork with subordinate sulfides (pyrite and chalcopyrite), showing propylitic alteration haloes overprinting a previous potassic alteration event (biotitization); (2) an overlying, kaolinized lithic-rich rhyolitic tuff; and (3) a layered opal deposit with preserved sedimentary structures. This vertical zonation, coupled with the distribution of the alteration assemblages, lead us to the interpretation of the whole as a porphyry-type deposit grading upwards to a barren, steam-heated, acid-leached, kaolinite blanket with a partially preserved silica sinter on top. Both the fluid inclusion study carried out on the veins and stockwork, and the stable isotopic analyses of the kaolinized bodies, suggest the presence of two major hydrothermal events. The older event is characterized by the occurrence of hot hypersaline fluids (up to 320°C and 36 wt% NaCl equivalents), likely of magmatic origin, closely associated with the emplacement of the underlying early Miocene porphyry-type deposit. The later event is characterized by the presence of cooler and dilute fluids (up to 140°C and 4 wt% NaCl equivalents) and by advanced argillic alteration close to the paleosurface. The calculated isotopic composition of water in equilibrium with the kaolinitic sequence plots close to and underneath the meteoric water line, partially overlapping the Los Humeros present-day geothermal fluids. This evidence coupled with the petrographic observations suggests that steam-heated phreatic waters altered the lithic-rich rhyolitic tuff. This would have occurred when acid vapors, exsolved from deeper hydrothermal fluids by boiling, reached the local paleowater table and condensed, after a sector collapse that changed the system from lithostatic to hydrostatic conditions.

Key words: argillic alteration, hydrothermal fluids, Ixtacamaxtitlán, kaolinite, Mexico, porphyry-type deposit, silica sinter, stockwork

Received 12 January 2004; accepted 4 August 2004

Corresponding author: Jordi Tritlla, Centro de Geociencias, Universidad Nacional Autónoma de México, Campus Juriquilla, Carretera Qro.-S.L.P. km 15,5, 76230, Santiago de Querétaro, Querétaro, Mexico.
Email: jordit@geociencias.unam.mx. Tel: 52-442-2381116. Fax: 52-442-2381100.

Geofluids (2004) **4**, 329–340

INTRODUCTION

Kaolinite can be produced by both hydrothermal alteration and weathering under tropical or sub-tropical wet climatic conditions. A supergene origin can be easily deduced when kaolinite masses are found *in situ* in lateritic profiles on sedimentary or metamorphic rocks, but when they are found on granitic or porphyrityc rocks, their origin may be uncertain. Hydrothermal activity associated with the late cooling of granite or hydrothermal circulation, induced by the presence of sub-volcanic intrusive rocks, may also generate extensive kaolinization. Detailed mapping, in addition to fluid inclusion studies in associated minerals (mainly quartz), and stable isotope studies of kaolinite are useful in

determining the origin of the kaolinite (e.g. Sheppard 1977; Alderton & Rankin 1983; Bird & Chivas 1988; Boulvais *et al.* 2000).

In this paper we present the geology of the Ixtacamaxtitlán kaolinite deposit and its relationship to a porphyritic intrusion. We also propose a genesis for this deposit based on stable isotope analyses of kaolinite (δD and δ^{18}O), as well as fluid inclusion analyses from a poorly mineralized stockwork developed in the porphyritic intrusion and intimately related to the kaolinite deposit. In addition, we present new $^{40}Ar/^{39}Ar$ geochronology for biotite in the potassic alteration recorded in the underlying porphyry intrusion in the area.

GEOLOGICAL SETTING

The Ixtacamaxtitlán sinter and kaolinite deposit is located in Puebla State in east-central Mexico (Fig. 1), at the intersection of the late Cenozoic Trans-Mexican Volcanic Belt (TMVB) with the Mesozoic sedimentary province of the Sierra Madre Oriental. The TMVB is an irregular belt that extends from Veracruz at the Gulf of Mexico to near Puerto Vallarta on the Pacific Ocean coast (Mooser 1972; Demant & Robin 1975; Demant 1981; Robin 1982; Verma 1987), and is considered to be a segment of the Circum-Pacific volcanic chain (Carrasco-Núñez *et al.* 1997). The TMVB is composed of a wide range of volcanic structures, including large stratovolcanoes, various silicic volcanic complexes, calderas and large monogenetic fields, and isolated silicic domes (Carrasco-Núñez *et al.* 1997). The magmatism is mainly calc-alkaline, producing rocks that range in composition from basalt to rhyolite (Carrasco-Núñez *et al.* 1997). For the most part, the TVMB is considered of Pliocene to Pleistocene–Holocene age. However, there are abundant andesitic volcanic rocks, and their sub-volcanic equivalents, of late Miocene age that are located in this province underlying the youngest and most obvious volcanic structures of the TMVB (Carrasco-Núñez *et al.* 1997). This late Miocene volcanism is not correlated with the older, mostly ignimbritic Sierra Madre Occidental Province (SMO), which is well defined to be Eocene-early Miocene in age (Demant *et al.* 1989). It appears that there is a hiatus between the late Miocene and the Plio-Quaternary episodes of volcanism. Ferrari *et al.* (1994) indicated that the transition between from the SMO to the TMVB occurred some time between 26 and 16 Ma.

The stratigraphy of the Ixtacamaxtitlán area can be separated into two main sequences: (1) a Mesozoic sedimentary rock sequence corresponding to the Sierra Madre Oriental; and (2) a sequence of late Cenozoic igneous extrusive rocks. Sporadically, minor plutonic rocks, mostly related to the Cenozoic extrusive rocks, affect the sedimentary sequence.

Geology of the Ixtacamaxtitlán deposit

Mesozoic sedimentary sequence

The Mesozoic sedimentary sequence in the study area corresponds to the Upper Tamaulipas Formation of Cretaceous age (Reyes-Cortés 1979). This formation is represented by a gray, medium layered limestone, with interbedded chert lenses and nodules, minor sandstones, and shales. This sequence is very limited in outcrop and is intensely folded by the Laramide orogeny (Fig. 1).

Cenozoic volcanic sequence

The Mesozoic sequence is discordantly overlain by late Cenozoic extrusive rocks, whose interrelations are still not well known. Following López-Hernández (1995), Carrasco-Núñez *et al.* (1997) and Morales-Ramírez (2002), two different volcaniclastic units are recognized in the study area, the Coyoltepec Pyroclastic Deposit and the Xaltipán Ignimbrite, respectively.

The Coyoltepec Pyroclastic Deposit (Carrasco-Núñez *et al.* 1997) is composed of two subunits. The lower Coyoltepec Pyroclastic Deposit is absent in the study area, but consists of a stratified sequence of surge deposits and massive, moderately indurated pyroclastic flow deposits with minor amounts of pumice and altered lithic clasts. The upper Coyoltepec Pyroclastic Deposit, which is the main unit outcropping in the study area, is a lithic rhyolite tuff composed of massive, indurated, coarse-gravel sized, lithic-rich pyroclastic flow deposits with pumice, andesitic fragments, free quartz, K-feldspar, plagioclase crystals, and subordinate amounts of limestone and shale clasts. The kaolinite deposit is mainly developed on this subunit (Fig. 1).

The Xaltipán Ignimbrite (López-Hernández 1995; Carrasco-Núñez *et al.* 1997) is mainly found in topographic depressions south of the study area. It consists of a very recent (0.45 ± 0.09 Ma; Carrasco-Núñez *et al.* 1997), pinkish to brownish-gray rhyolitic ignimbrite unit with different grades of welding, containing abundant pumice fragments, andesite lithic fragments, and small clasts of black obsidian (Fig. 1).

Both units were covered by a thin (up to 1 m) quaternary 'tegument' (Morales-Ramírez 2002), that only remains in small patches but is widespread outside the study area. This 'tegument' is composed of a very recent ash fall tuff rich in heavy minerals (mainly magnetite, apatite, and pyroxene).

Plutonic rocks

Very small Tertiary intrusive bodies are found outcropping in the region. The composition of these rocks is very variable, consisting of hornblende–biotite-bearing tonalites, quartz–plagioclase–hornblende–diorites, and some aphanitic diabase dikes (Carrasco-Núñez *et al.* 1997).

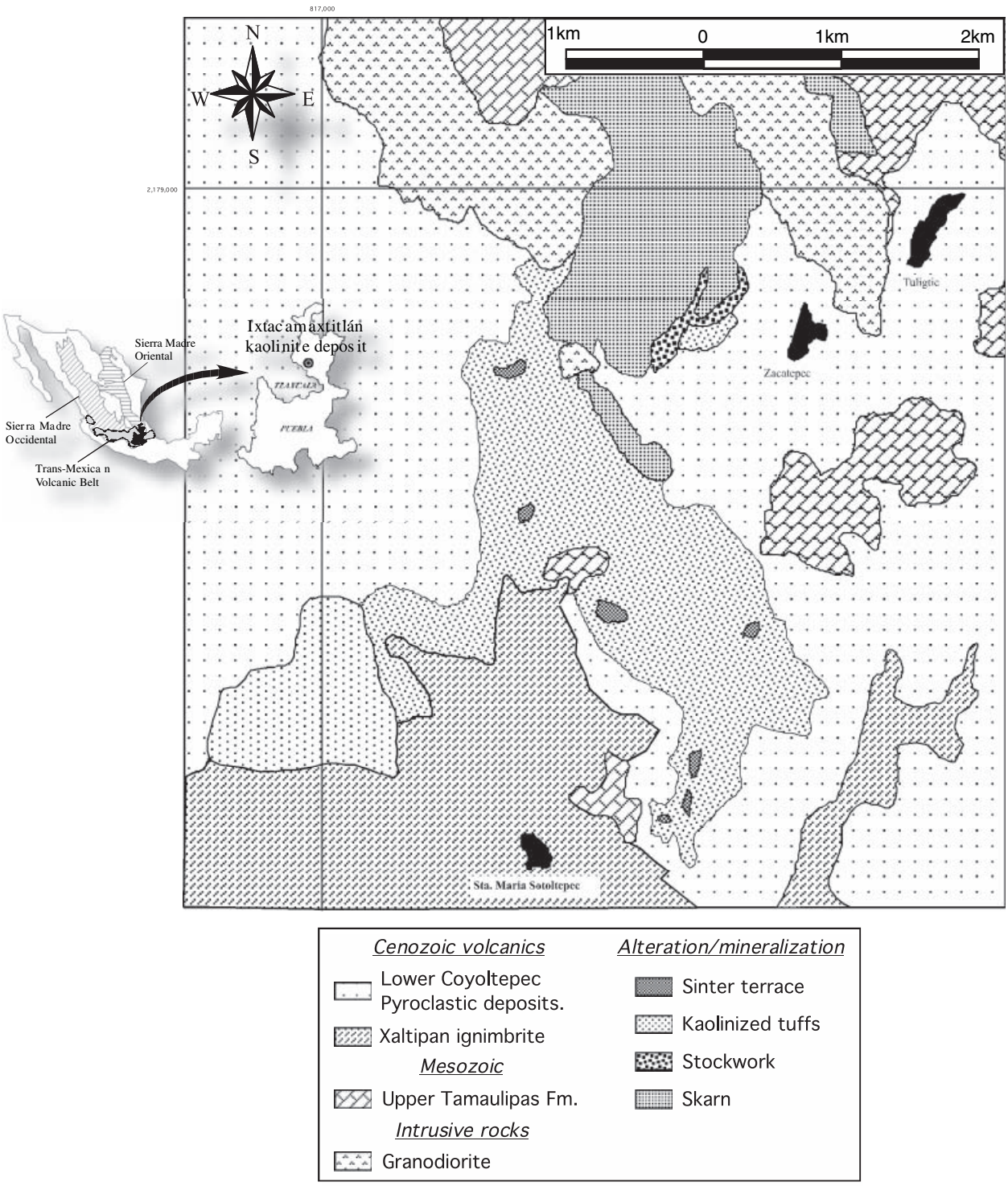

Fig. 1. Geological map of the Ixtacamaxtitlán area, modified from Morales-Ramírez (2002).

In Ixtacamaxtitlán, a hornblende–biotite-bearing granodiorite body, with porphyritic texture, intrudes both the Mesozoic Upper Tamaulipas Formation and the lower part of the upper Coyoltepec pyroclastic unit (Fig. 1). This granodiorite shows a porphyritic texture, with phenocrysts of quartz, plagioclase, K-feldspar, biotite, and pseudomorphous biotite after hornblende in a matrix of quartz, K-feldspar, and plagioclase. The contact between the granodiorite and the Mesozoic limestone is marked by the development of a prograde skarn. In a small

outcrop near the Zacatepec village (Fig. 1), the porphyritic granodiorite is crossed by a medium to dense network of quartz veins and veinlets; its upper part is marked by the complete replacement of feldspars by kaolinite, passing smoothly to the highly altered upper Coyoltepec pyroclastic subunit. Late mafic dikes (diabase), partially altered and with trachytic texture, are locally found crosscutting the granodiorite.

Hydrothermal events

In Ixtacamaxtitlán, we have found at least four different hydrothermal events affecting both the upper part of the porphyritic intrusion as well as the basal part of the upper Coyoltepec Pyroclastic deposit (Carrasco-Núñez *et al.* 1997).

Skarn

A small skarn is developed north of the studied area at the contact between the intrusion and the Upper Tamaulipas Formation limestone. This contact is very irregular, with blocks of the skarn enclosed within the magmatic rock, suggesting the presence of a magmatic-stopping setting. The resulting metasomatic rocks are of green to gray color, very fine grained and usually show very thin laminations. The mineralogy is mainly composed by calcite, grossularic garnet, hedenbergite, and subordinate quartz and calcite. Locally this contact has been mined for the very irregular accumulations of pyrite and sphalerite.

Veins and stockwork

Subvertical veins of quartz, chalcedony and subordinate sulfides (pyrite and minor chalcopyrite), up to 1.5 m thick, are found crosscutting the hornblende–biotite porphyry. These veins are mostly massive to banded, with sporadic cockade structures and idiomorphic quartz-lined vugs, containing highly altered fragments of the enclosing porphyry. The stockwork also crosscuts the intrusive rock (Fig. 2A), and is made up of an array of veinlets several decimeters long and few millimeters thick, composed of quartz, pyrite, minor chalcopyrite and rare sphalerite. The enclosing intrusive rock shows thin (up to a centimeter thick) propylitic haloes surrounding the quartz veinlets, grading outwards to a pervasive potassic alteration. This potassic alteration comprises replacement of magmatic amphibole crystals (hornblende) by a mesh of secondary biotite (Fig. 2B). A late, pervasive kaolinization of the feldspars affects the whole subvolcanic rock, still preserving the original magmatic texture.

Kaolinized rhyolitic tuff

There is a gradual increase in kaolinitic alteration upwards from the intrusive unit into the lithic-rich rhyolitic tuff, which is pervasively altered to a kaolin-rich secondary rock (Fig. 2C), with a maximum recognized thickness of about 50 m. The lower part of the kaolinized rhyolitic tuff is also crosscut by quartz veins grading upwards to opal veinlets, in continuity with both the granodiorite and the stockwork. The original tuff layering and some of the internal textures (laminations mainly) are well preserved throughout the sequence (Fig. 2D), and the original changes in composition are reflected in the very variable amounts of residual quartz and plagioclase left in the altered rock, grading from barely kaolinized bodies to full replacement.

Sporadically, some subconcordant opal-cemented breccias, containing fragments of highly silicified tuff, up to a few decimeters thick, appear scattered throughout the entire pyroclastic unit.

Silica sinter

The silica sinter unit is mainly eroded and only remnants occur on hill tops (Fig. 2C). The sinter consists of a crust, several meters thick, of laminated amorphous silica (opal), interbedded with small kaolin pods within vuggy horizons, composed of elongated cavities grossly parallel to the laminae (Fig. 2E). Some of the layers show primary structures that strongly suggest formation in a subaerial environment (Camprubí *et al.* 2001): bioturbation, imprints of vegetal remains and the abundance of polygonal cracking induced during gel desiccation (mud cracks; Fig. 2F), similar to those found in Buckskin Mountain, Nevada (Vikre 1985). This unit is commonly crosscut by subvertical thin opal veinlets, coupled with brecciation of the opal laminae, which could represent the feeder channels of the ascending hydrothermal solutions on their way to the paleosurface. In a single location we also found an accumulation of tightly packed, thin opal layers lacking any of the above structures. This tightly packed silica rock resembles the silica precipitates found at the bottom of some present-day hydrothermal pools (Hedenquist *et al.* 2000).

ANALYTICAL PROCEDURES

Fluid inclusions

A fluid inclusion study was undertaken to define the history of the vein-forming solutions. Standard and thick sections were used for petrographic examination. About 10 double-polished quartz wafers of 1 cm^2 were selected for microthermometric determinations. Microthermometric analyses were performed on a Linkam THMS-600 (Linkman Scientific Instruments Ltd.) heating–freezing stage calibrated with synthetic fluid inclusions including the triple point of distilled water (0.0°C), pure CO_2-bearing fluid inclusions (−56.6°C) and chemicals from the Merck Corporation. Accuracy in measurements is estimated about ±0.2°C for freezing runs and ±2°C for heating runs (Table 1). Microthemometric data were reduced using the MACFLINCOR software (Brown & Hagemann 1995).

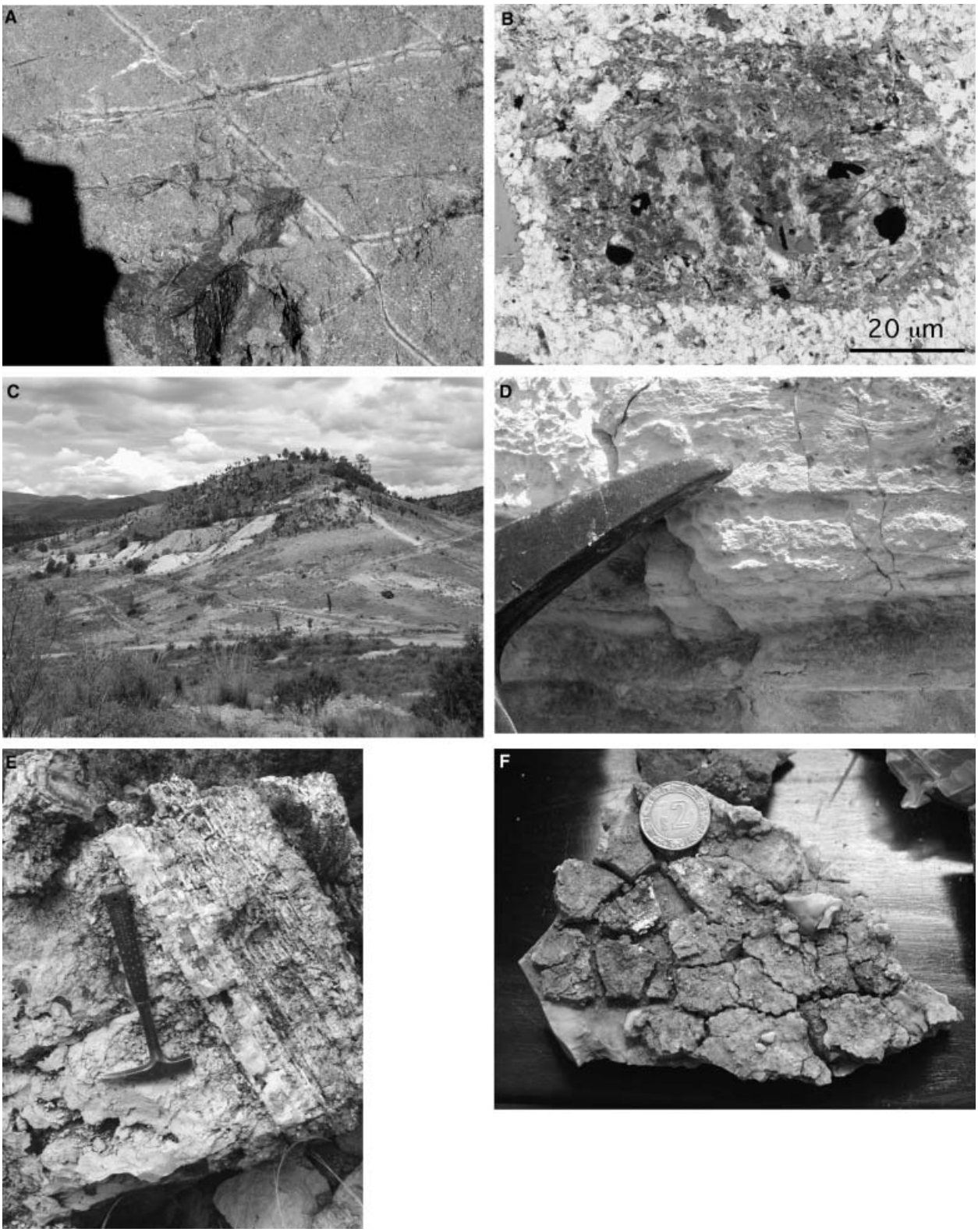

Fig. 2. (A) View of the stockwork crosscutting the porphyritic rock. (B) Porphyry rock, potassic alteration: pseudomorphic biotite after a former magmatic amphibole crystal (hornblende basal section) under polarized light. (C) Main sinter outcrop: contact between the highly kaolinized Coyoltepec pyroclastics, with a partially developed kaolinite quarry, covered by the sinter cap (with vegetation). (D) original tuff layering conserved in the pervasively altered Coyoltepec pyroclastic unit. (E) Close view of the highly porous sinter deposit and its lamination. (F) opal sinter: polygonal cracking induced during gel desiccation (mud cracks).

$^{40}Ar/^{39}Ar$ geochronology

Biotite separates from two different porphyritic granodiorite samples from the Ixtacamaxtitlán area were dated using the $^{40}Ar/^{39}Ar$ method (Fig. 3 and Table 1). Biotite mineral separates ranged in size between 250 and 180 μm and were produced using magnetic separation, heavy liquids and handpicking techniques to a purity of >99%. Samples were washed in acetone, alcohol and deionized water in an ultrasonic cleaner to remove dust and then re-sieved by hand using a 180-μm sieve.

Biotite samples IXT-SM-36A (1.0 mg) and IXT-SM-36B (8.8 mg) were packaged for irradiation in the central thimble facility at the TRIGA reactor (GSTR) at the US Geological Survey in Denver, CO, USA. The monitor mineral used in the package was Fish Canyon Tuff sanidine (FCT-3) with an age of 27.79 Ma (Kunk *et al.* 1985; Cebula *et al.* 1986) relative to MMhb-1 with an age of 519.4 ± 2.5 Ma (Alexander *et al.* 1978; Dalrymple *et al.* 1981). The type of container and the geometry of samples and standards is similar to that described by Snee *et al.* (1988).

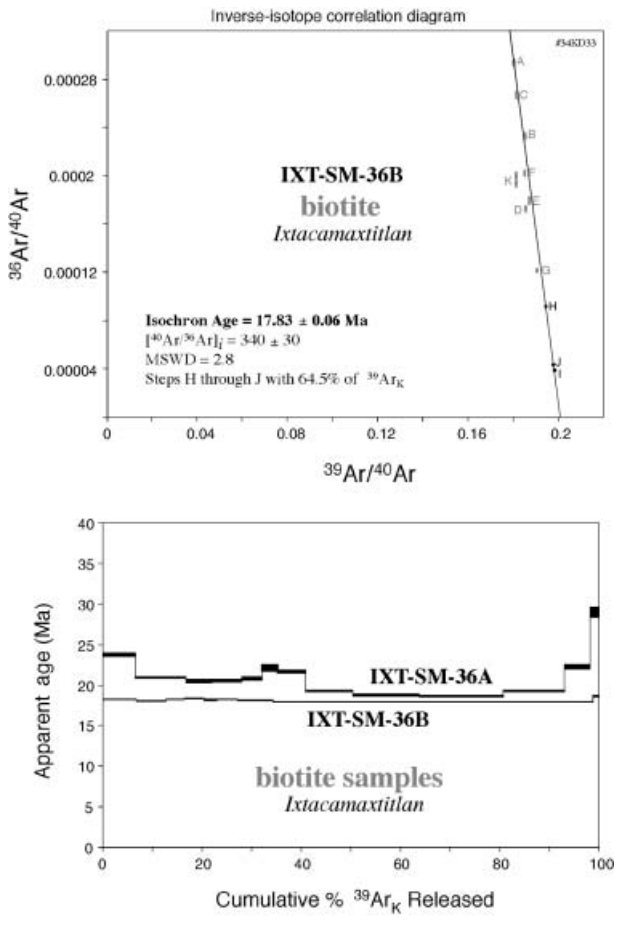

Fig. 3. (A) Isochron for the IXT-SM-36B biotite sample; (B) cumulative % ^{39}Ar released for samples IXT-SM-36 A and B.

All samples were analyzed at the US Geological Survey Thermochronology Lab in Denver, CO, using the $^{40}Ar/^{39}Ar$ step-heating method (Kunk *et al.* 2001).

The argon isotopic data were reduced using the computer program MASS SPEC (Deino 2001). We used the decay constants recommended by Steiger & Jäger (1977). Table 2 shows $^{40}Ar/^{39}Ar$ step-heating data and includes the identification of individual step, plateau, average, and total gas ages. An individual step age represents the apparent age obtained for a single temperature step analysis. Plateau ages are identified when three or more contiguous steps in the age spectrum agree in age, within the limits of analytical precision, and contain more than 50% of the $^{39}Ar_K$ released from the sample. The average ages are calculated from contiguous steps forming no plateau but containing more than 50% of the gas with the intention of obtaining the best age approximation for the sample. Total gas ages represent the age calculated from the addition of all of the measured argon peaks for all steps in a single sample. The total gas ages are roughly equivalent to conventional K–Ar ages. No analytical precision is calculated for total gas.

We have also calculated isochron ages using inverse-isotope correlation diagrams that plot $^{39}Ar/^{40}Ar$ against $^{36}Ar/^{40}Ar$ (Fig. 3). When reporting isochron ages we include the apparent age of the sample (calculated from the inverse of the *x*-axis intercept), the calculated initial $^{40}Ar/^{36}Ar$ ratio of the sample (the inverse of the *y*-axis intercept), the mean standard of weighted deviates (MSWD) a goodness-of-fit indicator of the data, the number of steps used in the age regression, and the percentage of $^{39}Ar_K$ they represent.

δD and $\delta^{18}O$ measurements of kaolinite

Sampling and cleaning

Samples from the altered pyroclastic unit were collected from outcrops and a small kaolinite quarry located underneath the main sinter outcrop. Clay-size fractions were obtained by gently crushing samples, followed by suspension and dispersion in distilled water. Sample purity was checked by X-ray diffraction (XRD) using a Bruker D5005 difractometer (40 kV and 30 mA), with a scanning rate of 0.04° and a incremental counting time of 3 sec (Dr Joaquín Bastida, Analyst). The main impurity detected in few samples is the presence of traces of alunite that could account for a small dispersion in the isotopic data.

Isotopic analyses

Hydrogen and oxygen isotopic compositions of kaolinite were analyzed at the Actlabs Laboratories in Ancaster, Canada, and at the Laboratorio de Isotopía Estable of the Universidad de Salamanca, Spain. H_2O and H_2 were evolved from clay minerals by placing them in a platinum

Table 1 Summary of data from fluid inclusions of the stockwork at the Ixtacamaxtitlán deposits.

FI type	Character	Trapped minerals	Host mineral	*n*	Th (°C)	Tm_i(°C)	Ts_{NaCl}	Salinity (wt% NaCl equivalents)
Poly-phase	Primary	Hematite	Quartz	87	240–320	–	240–281	31–36
Two-phase	Secondary	None	Quartz	15	140–150	−6	–	4

Table 2 $^{40}Ar/^{39}Ar$ step-heating data for biotite samples from Ixtacamaxtitlán porphyry deposit.

Step	Temperature (°C)	$\%^{39}Ar$ of total	Radiogenic yield (%)	$^{39}Ar_k$ (mol)	$^{40}Ar^*$ $^{39}Ar_k$	Apparent K/Ca	Apparent K/Cl	Apparent age (Ma)	Error (Ma)
IXT-SM-36A biotite ($J = 0.001969 \pm 0.25\%$; wt = 1.0 mg; #60KD33)									
A	900	6.7	69.8	1.04×10^{-14}	6.7054	33	8.3	23.72	±0.12
B	950	10.2	86.2	1.60×10^{-14}	5.8889	88	8.3	20.85	±0.07
C	1000	5.2	84.3	8.18×10^{-15}	5.7602	172	8.4	20.39	±0.11
D	1050	6.0	87.1	9.46×10^{-15}	5.7873	91	8.3	20.49	±0.10
E	1100	4.1	85.4	6.49×10^{-15}	5.8551	142	8.5	20.73	±0.11
F	1150	2.9	80.7	4.55×10^{-15}	6.2390	186	8.8	22.08	±0.18
G	1200	5.7	86.5	8.93×10^{-15}	6.1150	813	8.4	21.64	±0.09
H	1225	9.5	88.4	1.49×10^{-14}	5.4302	100 000	8.4	19.23	±0.06
I	1250	13.5	76.6	2.11×10^{-14}	5.2878	1923	8.2	18.73	±0.07
J	1276	16.9	86.3	2.65×10^{-14}	5.2550	12 500	8.2	18.61	±0.05
K	1300	12.3	86.4	1.92×10^{-14}	5.4254	350	8.4	19.22	±0.06
L	1325	5.3	77.4	8.23×10^{-15}	6.2767	709	8.8	22.21	±0.13
M	1350	1.6	65.5	2.59×10^{-15}	8.1999	53	10.0	28.96	±0.33
Total gas		100.0						20.26	
IXT-SM-36B biotite ($J = 0.001990 \pm 0.25\%$; wt = 8.8 mg; #34KD33)									
A	900	6.8	91.3	1.07×10^{-13}	5.0763	82	8.5	18.18	±0.03
B	950	6.0	93.1	9.34×10^{-14}	5.0286	134	8.6	18.01	±0.03
C	1000	3.6	92.1	5.71×10^{-14}	5.0821	112	8.5	18.20	±0.03
D	1050	4.0	94.9	6.28×10^{-14}	5.1173	98	8.6	18.32	±0.03
E	1100	2.8	94.7	4.31×10^{-14}	5.0708	102	8.6	18.16	±0.03
F	1150	4.1	94.0	6.44×10^{-14}	5.0825	136	8.5	18.20	±0.03
G	1200	7.1	96.4	1.11×10^{-13}	5.0630	206	8.6	18.13	±0.03
H	1250	20.8	97.3	3.26×10^{-13}	5.0023	338	8.8	17.91	±0.02
I	1300	29.2	98.8	4.57×10^{-13}	4.9834	429	8.8	17.84	±0.02
J	1350	14.5	98.7	2.27×10^{-13}	4.9987	224	8.7	17.90	±0.02
K	1400	1.2	94.2	1.82×10^{-14}	5.1942	44	8.8	18.60	±0.05
Total gas		100.0						17.98	
Average age								17.88	±0.06

64.5% of gas released in steps H–J.
Ages calculated assuming an initial $^{40}Ar/^{36}Ar = 295.5 \pm 0$.
All precision estimates are at the one sigma level of precision.
Ages of individual steps do not include error in the irradiation parameter *J*.
No error is calculated for the total gas age.

crucible and heating under vacuum at temperatures >1500°C, following the method of Godfrey (1962) modified by Jenkin (1988). The water was converted to hydrogen gas by reduction over hot depleted Uranium. Oxygen was extracted from the clays following the procedure of Clayton & Mayeda (1963) using ClF_3 as reactant (Borthwick & Harmon 1982). The hydrogen and oxygen isotope data are reported in the normal δ-notation relative to V-SMOW (Table 3). Isotope measurements were performed using the spectrometers Finnigan Mat 251 (Actlabs) and VG-Sira-II (Universidad de Salamanca). Two aliquots were obtained for some selected samples and analyzed in both laboratories to ensure a comparable set of analyses.

RESULTS

Fluid inclusions

Clusters of fluid inclusions (10–40 μm) were found in most stockwork and vein quartz, both randomly distributed within the crystals (primary) and in planes that crosscut the

Sample	$\delta^{18}O_{kaolinite}$	$\delta D_{kaolinite}$	$\delta^{18}O_W$ (140°C)	δD_W (140°C)	$\delta^{18}O_W$ (100°C)	δD_W (100°C)
IXS-7	20.5	−59.0	8.75	−41.4	5.5	−37.8
IXS-8	20.2	−86.0	8.45	−68.4	5.2	−64.8
IXS-9	20.1	−62.0	8.35	−44.4	5.05	−40.8
IXT-31	12.1	−76.0	0.4	−58.4	−2.9	−54.8
IXT-37	10.6	−67.0	−1.15	−49.4	−4.5	−45.8
IXT-38	14.4	−62.0	2.7	−44.4	−0.7	−40.8
DO-1	16.2	−115.0	4.5	−97.5	1.15	−93.9
DO-5	13.1	−89.3	1.4	−71.7	−1.9	−68.1
DO-7	14.7	−79.4	2.9	−61.8	−0.4	−58.2
DO-8	10.2	−61.8	−1.6	−44.2	−4.9	−40.6
DO-9	15.0	−61.4	3.3	−43.8	−0.1	−40.2
DO-10	14.8	−78.9	3.1	−61.3	−0.3	−57.7
DO-11	17.8	−75.6	6.1	−58.0	2.8	−54.5
DO-12	17.1	−75.6	5.4	−58.0	2.1	−54.4
DO-13	17.4	76.2	5.7	−58.6	2.4	−55.0
DO-15	16.6	−102.0	4.9	−84.1	1.6	−80.5
DO-19	15.5	−54.8	3.8	−37.2	0.5	−33.6
DO-20	20.4	−69.8	8.7	−52.2	5.4	−48.6
DO-21	18.4	−41.2	6.7	−23.6	3.4	−20.0
DO-22	17.7	−38.2	5.6	−20.6	2.7	−17.0
DO-23	16.8	−105.0	5.1	−87.0	1.8	−83.4

Table 3 Oxygen and hydrogen isotopic composition for kaolinite samples and water in equilibrium with them at 140 and 100°C.

growth bands (secondary). Primary fluid inclusions in vein quartz are three- to poly-phase (liquid + vapor bubble + halite ± hematite), usually between 10 and 30 μm in size, with a 0.8 visual estimation of the degree of filling (liquid + halite/vapor ratio). The effect of post-trapping changes (necking-down mainly) affecting primary polyphase fluid inclusions is evident in some samples, so those inclusions were carefully avoided for microthermometric analyses, although, it is noteworthy that some of these necked fluid inclusions have a 'hook-shaped' morphology, similar to the fluid inclusions described by Vityk & Bodnar (1995). Our preliminary data for primary fluid inclusions indicates that their minimum homogenization temperatures are between 240 and 320°C with temperatures of halite dissolution (T_{fh}) between 180 and 281°C and corresponding salinities between 31 and 36 wt% NaCl equivalents.

Secondary two-phase fluid inclusions (aqueous fluid + vapor bubble), of 10–50 μm in size and a visual degree of filling between 0.8 and 0.9, are scarce within the quartz crystals of the stockwork. These fluid inclusions have a first melting temperature (eutectic) located around −26°C, suggesting the presence of small quantities of $CaCl_2$ in the hydrothermal solutions. Ice-melting temperatures are around −6°C, with a calculated salinity around 4 wt% NaCl equivalents. Homogenization temperature by bubble shrinkage cluster between 140 and 150°C.

$^{40}Ar/^{39}Ar$ geochronology

Gas obtained from biotite sample IXT-SM-36B does not form a plateau. The isochron age for this sample (Fig. 3A) is 17.83 ± 0.06 Ma (Fig. 4; $^{40}Ar/^{36}Ar_i = 340 \pm 30$, MSWD = 2.8; 64.5% of $^{39}Ar_K$), within analytical error of the calculated average age at 17.88 ± 0.06 Ma, assuming a $^{40}Ar/^{36}Ar$ initial value of 295.5. From the isochron calculation it is possible to estimate an $^{40}Ar/^{36}Ar$ initial value of 340 ± 30, perhaps indicating the presence of small amounts of excess argon in the crystal lattice of the biotite. Therefore, the isochron age at 17.83 ± 0.06 Ma is the best

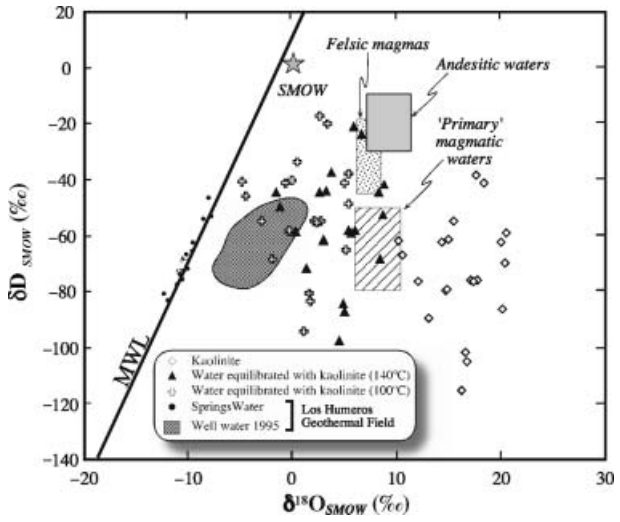

Fig. 4. $\delta^{18}O$ versus δD plot for the kaolinite analyses. MWL: meteoric water line; SMOW: standard mean ocean water composition. The 'primary' magmatic water box is drawn after Sheppard *et al.* (1969) and Taylor (1974) and Sheppard (1986), the box of felsic magmatic waters comes from Taylor (1992), and the andesitic water box after Giggenbach (1992a,b).

estimation for the time at which the biotite sample cooled below its argon closure temperature of 280 ± 40°C (Harrison *et al.* 1985). This age constrains the time of potassic alteration (biotitization) observed in the porphyritic granodiorite unit in the Ixtacamaxtitlán area.

Biotite sample IXT-SM-36A presents a very disturbed age spectrum with a classic U-shape suggesting the presence of excess argon (Fig. 3B), and the total gas age at ~20 Ma probably overestimates the age of the biotite because of the presence of excess argon. The best estimate of age will be the age of the youngest temperature step (step J) at 18.61 ± 0.05 Ma (see Table 1), and this is the maximum possible age for this biotite sample, in agreement with the result from IXT-SM-36B.

Stable isotopes

The kaolinite δD values range between −59 and −86‰ while δ^{18}O ranges from + 10.6 to + 20.4‰. Proposed kaolinite–water fractionation equations diverge considerably, and after the examination of the different equations and published discussions (Savin & Epstein 1970; Lawrence & Taylor 1971; O'Neil & Kharaka 1976; Suzuoki & Epstein 1976; Land & Dutton 1978; Savin & Lee 1978; Marumo *et al.* 1980; Liu & Epstein 1984), the empiric kaolinite–water hydrogen fractionation factors of Marumo *et al.* (1980) was chosen. These empiric fractionation factors were proposed for a similar geological setting and temperature conditions to the Ixtacamaxtitlán deposit. In order to work with a self-coherent set of data, we also choose the Land & Dutton (1978) empirical kaolinite–water oxygen fractionation equation.

To establish comparisons with present-day fluids in a similar setting, we used the available data for D and O isotopic composition of meteoric and hydrothermal waters of the Los Humeros geothermic field (Fig. 4; González-Partida *et al.* 2001), located a few kilometers away from the Ixtacamaxtitlán deposit and at the same present-day elevation. Groundwater from springs plot around the meteoric water line, with δD values between −82.6 and −52.7‰, peaking around −67‰ which is comparable to local precipitation values in the region (Fig. 4). Water sampled from hydrothermal wells mainly show similar δD values to meteoric waters, but δ^{18}O compositions are heavier, having a general trend suggesting a mixing between meteoric and δ^{18}O-evolved waters by water–rock interaction (González-Partida *et al.* 2001).

The hydrogen isotopic composition of kaolinite samples from Ixtacamaxtitlán is similar to the composition of the present-day local meteoric waters, where only three data points have slightly lower values (Fig. 4). In addition, the calculated δD compositions for hydrothermal waters in equilibrium with kaolinite between 100 and 140°C are comparable to, and partially overlap, the composition of the present-day hydrothermal waters sampled at the Los Humeros geothermal field. The oxygen isotopic composition of both kaolinite and the calculated hydrothermal water in equilibrium with it shows a marked shift to heavier oxygen isotopic compositions, with the lighter oxygen calculated waters also overlapping the Los Humeros hydrothermal water compositions. This O-shift is a possible consequence of the original oxygen isotopic composition of the rhyolitic tuff, where the dispersion of data can also probably reflect different water to rock ratios that could be controlled by local variations in permeability.

DISCUSSION

The high temperatures and salinities (up to 320°C, without pressure correction and 36 wt % NaCl equivalents) recorded for the primary (poly-phase) fluid inclusions found in vein quartz and in the stockwork, can be easily related to the high-temperature potassic alteration that affects the porphyritic intrusive rocks around the vein network. The presence of a pervasive, but selective, biotitization in the host rock and its proximity to the kaolinized sequence and sinter, suggests that both the magmatic rocks and the stockwork were originally emplaced at deeper levels. Moreover, following Vityk & Bodnar (1995), the 'hook-shaped' morphology displayed by some primary poly-phase fluid inclusions can be interpreted as the result of an isothermic decompression path, which caused the partial necking of the inclusions because of inner overpressure. Such decompression can only be because of the uplifting of the magmatic body and the associated mineralized deposit. All these characteristics suggest that the exposed deposit could be the exhumed upper part of a porphyry-type deposit.

The argillic and advanced argillic alteration assemblage affecting the upper Coyoltepec Pyroclastic deposit, mainly composed of kaolinite, with traces of alunite and residual quartz and plagioclase, directly caps the porphyry-type deposit and is also responsible for the partial alteration of the feldspars of the porphyry rock. The presence of secondary fluid inclusions with contrasting low salinity (4 wt% NaCl equivalents) and temperatures (≈140°C) in the stockwork, the clear meteoric origin of water in equilibrium with the kaolinitic sequence, and the occurrence of the alteration assemblage underneath a silica sinter suggests a near-surface formation for whole. The ascending fluids would have been channelized by the stockwork structure and fractures. Boiled-off steam and acid volatiles, when condensating into cool groundwater would form steam-heated acid fluids that caused argillic and advanced argillic alteration assemblages. This scenario is commonly found at the top of both high- and low-sulfidation epithermal deposits and present-day analogous geothermal systems

(Sillitoe 1993; Hedenquist *et al.* 2000). Moreover, stratabound silicified horizons are found developed in permeable lithologic units, similar to the ones described by Muntean *et al.* (1990) in conglomerates at the Pueblo Viejo deposit in Dominican Republic. These stratabound silicified horizons probably formed by cooling of the ascending fluids after mixing with local groundwater.

The kaolinite blanket is topped by a porous silica sinter indicating the rapid cooling of the boiling fluid after its ascent to the paleosurface. The sedimentary structures found in the opal layers indicate that these formed in a hot-spring pool, possibly controlled by climate seasonality. Alternate periods of wet seasons, with hydrothermal activity and deposition of silica, and dry seasons, with the subsequent water table retreat and sediment desiccation, would account for polygonal cracking in the silica gel, a widespread feature in these deposits. The thickness of the kaolinized bodies (up to 50 m thick) is probably a result of the arid climate during the emplacement of the hydrothermal system that, also, accounted for the seasonality of the water pool and sinter terrace. Descent of the water table during sinter-forming hydrothermal activity resulted in acid leaching beneath the sinter terrace. This mechanism was already invoked by Vikre (1985) in respect to the sinter formations at the Buckskin Mountain deposit in Nevada. The presence in isolated outcrops of non-porous, tightly packed silica crusts resembling the present-day precipitates at the bottom of some hydrothermal pools, suggest either the former existence of a big single hydrothermal pool or the presence of several discharging areas and pools.

During the past few years, a connection between high-sulfidation epithermal deposits and porphyry-type deposits has been established, with the latter separated from an advanced argillic lithocap by as much as 1 km (Hedenquist *et al.* 2000). The presence of a kaolinite blanket at Ixtacamaxtitlán topping and partially affecting a porphyry body without an epithermal vein deposit as a link between them, points to either a rapid erosion because of the uplift of the whole deposit or a sector collapse of a volcanic edifice. These processes could have caused the telescoping of the magmatic-hydrothermal system with a superficial paleoaquifer developed within the porous lithic-rich rhyolitic tuff of the Coyoltepec pyroclastic unit. Syn-hydrothermal retreat of the water table produced the overprinting of the advanced argillic alteration over the former, high-temperature potassic alteration event in the porphyry-type deposit. Some of the aspects of the low-temperature stage of alteration, such as the shallow argillic alteration, the silica sinter on top, and the composition of the secondary fluid inclusions, could correspond to part of a low-sulfidation epithermal deposit. However, as no other characteristics favoring such an interpretation were found, we consider that it is not fully proven that the above structures actually correspond to an actual epithermal deposit.

The porphyritic granodiorite unit at Ixtacamaxtitlán contains two generations of biotite: (1) magmatic biotite that resulted from the crystallization of the granodiorite intrusion, and (2) secondary biotite, formed by the potassic alteration event as a result of the hydrothermal activity triggered by the intrusion. The age of this pervasive potassic alteration process is well constrained by the biotite Ar–Ar isochron age at 17.83 ± 0.06 Ma (Fig. 3). Most of this second generation of biotite appears to be the result of pseudomorphic replacements after hornblende. Based on the fluid inclusion work, we estimated minimum temperatures between 240 and 320°C for the hydrothermal system affecting the intrusion. These temperatures are compatible with forming a second generation of biotite as the argon closure temperature of biotite (280 ± 40°C) must have been exceeded. The primary magmatic biotite was therefore reset under these temperatures. In a porphyry system, the crystallization of the shallow intrusion and the subsequent alteration processes would be broadly synchronous. We propose that the age of the biotite associated to the potassic alteration would actually be only slightly younger than the crystallization age of the granodiorite intrusion. In addition, the overprinting of the kaolinitic alteration as a result of the collapse of the hydrothermal system suggests that this age at 17.83 ± 0.06 Ma can be taken as the maximum possible age for the formation of the argillic and advanced argillic assemblages and the sinter deposits.

CONCLUSIONS

Geological and isotopic evidence indicate that a single hydrothermal system, evolving over space and time, was responsible for the formation of a poorly developed porphyry-type deposit, a kaolinite cap and the sinter terrace at the Ixtacamaxtitlán deposit. The system evolved from magmatic to meteoric water domination. A dominant magmatic component, trapped as primary, hypersaline fluid inclusions within the quartz veins and stockwork, belonging to the porphyry-type stage, is interpreted to have been responsible for the potassic alteration affecting the intrusive rock. Meteoric water incursion was the result of either a sector collapse or a rapid erosion event because of the uplifting of the whole deposit. This caused the subsequent shift to hydrostatic conditions, causing the decompression of the deposit as recorded in the fluid inclusion textures. Boiling of ascending fluids and the subsequent condensation of boiled-off acid-rich steam into groundwater would account for the formation of argillic and advanced argillic alteration assemblages at shallow depth. Also, the discharge of hydrothermal fluids at a hot-spring environment would account for the formation of silica sinters. Telescoping of the argillic alteration zone over the porphyry-type deposit probably occurred by the retreat of the water table during the waning stages of the hydrothermal system.

It is likely that the telescoped porphyry-type and kaolinite deposits were both produced by a single event of hydrothermal activity triggered by the host subvolcanic rocks, as described for deposits of the Coromandel Peninsula in New Zealand (Brathwaite *et al.* 2001; Simpson *et al.* 2004).

ACKNOWLEDGEMENTS

This study was financed by UNAM-PAPIIT projects IN115999 and IN114002, and CONACyT projects J32506-T and G35442-T. Specials thanks are devoted to Ing. Adalberto Terrazas, Dr Esteban Cardellach and Dr Joaquín Bastida for his help during the development of this project. Alexander Iriondo would like to thank Michael Kunk for providing access and guidance to perform the $^{40}Ar/^{39}Ar$ geochronology studies at the US Geological Survey Thermochronology Lab in Denver. We also thank Prof. Bruce Yardley and Dr Richard Herrington for their help in improving the paper.

REFERENCES

Alderton DHM, Rankin AH (1983) The character and evolution of hydrothermal fluids associated with the kaolinized St. Austell granite, SW England. *Journal of the Geological Society*, **140**, 297–309.

Alexander EC Jr, Mickelson GM, Lanphere MA (1978) Mmhb-1: a new $^{40}Ar/^{39}Ar$ dating standard. In: *Short Papers of the Fourth International Conference, Geochronology, Cosmochronology, and Isotope Geology* (ed. Zartman RE). *US Geological Survey Open-File Report*, **78-701**, 6–8.

Bird MI, Chivas AR (1988) Stable-isotope evidence for low-temperature kaolinite weathering and post-formational hydrogen-isotope exchange in Permian kaolinites. *Chemical Geology*, **72**, 249–65.

Borthwick J, Harmon RS (1982) A note regarding ClF_3 as an alternative to BrF_5 for oxygen isotope analysis. *Geochimica et Cosmochimica Acta*, **46**, 1665–8.

Boulvais P, Vallet JM, Estéoule-Choux J, Fourcade S, Martineau F (2000) Origin of kaolinization in Brittany (NW France) with emphasis on deposits over granite: stable isotopes (O, H) constraints. *Chemical Geology*, **168**, 211–23.

Brathwaite RL, Simpson MP, Faure K, Skinner DNB (2001) Telescoped porphyry Cu–Mo–Au mineralisation, advanced argillic alteration and quartz–sulphide–gold–anhydrite veins in the Thames District, New Zealand. *Mineralium Deposita*, **36**, 623–40.

Brown PE, Hagemann SG (1995) MACFLINCOR: a computer program for fluid inclusion data reduction and manipulation. In: *Fluid Inclusions in Minerals: Methods and Application* (eds De Vivo B, Frezzotti ML), pp. 231–50. Short Course of the Working Group (IMA) 'Inclusions in Minerals', Department of Geological Sciences, Virgina Tech, Blacksburg, Virginia, USA.

Camprubí A, Tritlla J, Corona-Esquivel R, Centeno E, Terrazas A (2001) The hydrothermal sinter and kaolinite–Au–Ag deposits of Ixtacamaxtitlán (Puebla, Mexico): preliminary research. In: *Mineral Deposits at the Beginning of the 21st Century* (eds Pietrzynski A *et al.*), pp. 711–4. Swets & Zeitlinger Publishers, Lisse.

Carrasco-Núñez G, Gómez-Tuena A, Lozano L (1997) Geologic Map of Cerro Grande Volcano and Surrounding Area, Central Mexico. *Geological Society of America, Map and Chart Series*, **CH 081**, 10.

Cebula GT, Kunk MJ, Mehnert HH, Naeser CW, Obradovich JD, Sutter JF (1986) The Fish Canyon Tuff: a potential standard for the $^{40}Ar/^{39}Ar$ and fission track dating methods. *Terra Cognita*, **6–2**, 140.

Clayton RN, Mayeda TK (1963) The use of bromine pentafluoride in the extraction of oxygen from oxides and silicates for isotopic analysis. *Geochimica et Cosmochimica Acta*, **27**, 43–52.

Dalrymple GB, Alexander EC, Lanphere MA, Kraker GP (1981) Irradiation of samples for $^{40}Ar/^{39}Ar$ dating using the Geological Survey TRIGA reactor. *US Geological Survey Professional Paper*, **1176**, 55.

Deino AL (2001) Users manual for MASS SPEC v. 5.02. *Berkeley Geochronology Center Special Publication*, **1**, 119.

Demant A (1981) L'Axe néovolcanique tansmexicain-étude volcanologique et petrograpie- signification géodynamique. PhD Thesis, Université d'Aix-Marseille, 259 pp.

Demant A, Robin C (1975) Las fases del vulcanismo en México: una síntesis en relación con la evolución geodinámica desde el Cretácico. *Revista del Instituto de Geología, Universidad Nacional Autónoma de México*, **1**, 70–82.

Demant A, Cochemé J, Delpretti P, Piguet P (1989) Geology and petrology of the Tertiary volcanics of the northwestern Sierra Madre Occidental, Mexico. *Bulletin de la Société Géologique de France*, **8–4**, 737–48.

Ferrari L, Garduño VH, Pasquarè G, Tibaldi A (1994) Volcanic and tectonic evolution of central Mexico: Oligocene to present. *Geofísica Internacional*, **33–3**, 91–105.

Giggenbach WF (1992a) Magma degassing and mineral deposition in hydrothermal systems along convergent plate boundaries. *Economic Geology*, **87**, 1927–44.

Giggenbach WF (1992b) Isotopic shifts in waters from geothermal and volcanic systems along convergent plate boundaries and their origin. *Earth and Planetary Science Letters*, **113**, 495–510.

Godfrey JD (1962) The deuterium content of hydrous minerals from the East-Central Sierra Nevada and Yosemite National Park. *Geochimica et Cosmochimica Acta*, **26**, 1215–45.

González-Partida E, Tello-Hinojosa E, Pal-Verma M (2001) Interacción agua geotérmica-manantiales en el campo geotérmico de Los Humeros, Puebla, México. *Ingeniería Hidráulica de México*, **XVI**, 185–94.

Harrison TM, Duncan I, McDougall I (1985) Diffusion of ^{40}Ar in biotite: temperature, pressure and compositional effects. *Geochimica et Cosmochimica Acta*, **49**, 2461–8.

Hedenquist JW, Arribas A, Gonzalez-Urien E (2000) Exploration for epithermal gold deposits. In: *Gold in 2000*, (eds Hagemann SG, Brown PE). *Reviews in Economic Geology*, **13**, 245–77.

Jenkin GRT (1988) Stable isotope studies in the caledonides of S.W. Connemara, Ireland. PhD Thesis, University of GlasgowGlasgow, UK.

Kunk MJ, Sutter JF, Naeser CW (1985) High-precision $^{40}Ar/^{39}Ar$ Ages of Sanidine, Biotite, Hornblende, and Plagioclase from the Fish Canyon Tuff, San Juan Volcanic Field, south-central Colorado. *Geological Society of America Abstracts with Programs*, **17**, 636.

Kunk MJ, Winick JA, Stanley JO (2001) $^{40}Ar/^{39}Ar$ age-spectrum and laser fusion data for volcanic rocks in west central Colorado. *US Geological Survey, Open-File Report*, **01-472**, 94.

Land LS, Dutton SP (1978) Cementation of a Pennsylvanian deltaic sandstone; isotopic data. *Journal of Sedimentary Petrology*, **48**, 1167–76.

Lawrence JR, Taylor HP Jr (1971) Deuterium and oxygen 18 correlation: clay minerals and hydroxides in Quaternary soils compared to meteoric waters. *Geochimica et Cosmochimica Acta*, **35**, 993–1003.

Liu KK, Epstein S (1984) The hydrogen isotope fractionation between kaolinite and water. *Isotope Geoscience*, **2**, 335–50.

López-Hernández A (1995) Estudio regional volcánico y estructural del campo geotérmico de Los Humeros, Pue., Mexico. *Geotermia. Revista Mexicana de Geoenergía*, **11-1**, 17–36.

Marumo K, Nagasawa K, Kuroda Y (1980) Mineralogy and hydrogen isotope geochemistry of clay minerals in the Ohnuma Geothermal area, Northeastern Japan. *Earth and Planetary Science Letters*, **47**, 255–62.

Mooser F (1972) The Mexican Volcanic Belt: Structure and tectonics. *Geofísica Internacional*, **12**, 55–70.

Morales-Ramírez JM (2002) Geología y metalogénia del deposito de Au–Ag–caolín de Ixtacamaxtitlán (Edo. de Puebla, México). Tesis de Licenciatura, Facultad de Ingeniería, Universidad Nacional Autónoma de México, 153 pp. (see Map 1).

Muntean JL, Kesler SE, Russell N, Polanco J (1990) Evolution of the Monte Negro acid sulfate Au–Ag deposit, Pueblo Viejo, Dominican Republic: important factors in grade development. *Economic Geology*, **85**, 1738–58.

O'Neil JR, Kharaka YK (1976) Hydrogen and oxygen isotope exchange reactions between clay minerals and water. *Geochimica et Cosmochimica Acta*, **40**, 241–6.

Reyes-Cortés M (1979) Geología de la Cuenca de Oriental, Estados de Puebla, Veracruz y Tlaxcala. *Colección Científica SEP-INAH*, **71**, 62.

Robin C (1982) Relations volcanologie–magmatologie–géodynamique: application au passage entre volcanismes alcalin et andésitique dans le sud Mexicain (Axe Trans-Mexicain et Province Alcaline Orientale). PhD Thesis, Université Clermont-Ferrand, 503 pp.

Savin SM, Epstein S (1970) The oxygen and hydrogen isotope geochemistry of clay minerals. *Geochimica et Cosmochimica Acta*, **34**, 25–42.

Savin SM, Lee M (1978) Isotope studies of phyllosilicates. In: *Hydrous Phyllosilicates (Exclusive of Micas)* (ed. Bailey SW). *Reviews in Mineralogy*, **19**, 189–223.

Sheppard SMF (1977) The Cornubian batolith, SW England: D/H and $^{18}O/^{16}O$ studies of kaolinite and other alteration minerals. *Journal of the Geological Society*, **133**, 573–91.

Sheppard SMF (1986) Characterization and isotopic variation in natural waters. In: *Stable isotopes in high temperature geological processes* (ed. Ribbe PH). *Mineralogical Society of America*, **16**, 1–40.

Sheppard SMF, Nielsen RL, Taylor HP Jr (1969) Oxygen and hydrogen isotope ratios of clay minerals from porphyry copper deposits. *Economic Geology*, **64**, 755–77.

Sillitoe RH (1993) Epithermal models: genetic types, geometrical controls and shallow features. *Geological Association of Canada Special Papers*, **40**, 403–17.

Simpson MP, Mauk JL, Kendrick RG (2004) Telescoped porphyry-style and epithermal veins and alteration at the central Maratoto valley prospect, Hauraki Goldfield, New Zealand. *New Zealand Journal of Geology and Geophysics*, **47**, 39–56.

Snee LW, Sutter J.F, Kelly WC (1988) Thermochronology of economic mineral deposits: Dating the stages of mineralization at Panasqueira, Portugal, by high precision $^{40}Ar/^{39}Ar$ age spectrum techniques on muscovite. *Economic Geology*, **83**, 335–54.

Steiger RH, Jäger E (1977) Subcommission on geochronology: convention on the use of decay constants in geo- and cosmochronology. *Earth and Planetary Science Letters*, **36**, 359–63.

Suzuoki T, Epstein S (1976) Hydrogen isotope fractionation between OH-bearing minerals and water. *Geochimica et Cosmochimica Acta*, **40**, 1229–40.

Taylor HP Jr (1974) The application of oxygen and hydrogen isotope studies to the problem of hydrothermal alteration and ore deposition. *Economic Geology*, **69**, 843–83.

Taylor BE (1992) Degassing of H_2O from rhyolite magma during eruption and shallow intrusion, and the isotopic composition of magmatic water in hydrothermal systems. In: *Extended Abstracts, Japan–US Symposium on Magmatic Contributions to Hydrothermal Systems* (ed. Hedenquist JW). *Geological Survey of Japan Reports*, **279**, 190–4.

Verma SP (1987) Mexican Volcanic Belt (Preface). In: *Mexican Volcanic Belt, Part 1* (ed. Verma SP). *Geofísica Internacional*, **24**, 7–19.

Vikre PG (1985) Precious metal vein systems in the National district, Humboldt County, Nevada. *Economic Geology*, **80**, 360–93.

Vityk MO, Bodnar MJ (1995) Textural evolution of synthetic fluid inclusions in quartz during re-equilibration, with applications to tectonic reconstructions. *Contributions to Mineralogy and Petrology*, **121**, 309–23.